Ceramics International xxx (xxxx) xxx

Contents lists available at ScienceDirect

Ceramics International

journal homepage: www.elsevier.com/locate/ceramint

5-fluorouracil and curcuminoids extract from *Curcuma longa* L. loaded into nanohydroxyapatite as a drug delivery carrier for SKOV-3 and HepG2 cancer cells treatment

Thu Phuong Nguyen [a,**], Sławomir Wilczewski [b,c], Jakub Lewandowski [d], Agnieszka Majkowska-Pilip [e], Kinga Żelechowska-Matysiak [e], Dorota Nieciecka [f], Waldemar Studziński [b], Sunday Joseph Olusegun [f], Marcin Syczewski [g,h], Michael Giersig [c], Thi Mai Thanh Dinh [i], Paweł Krysiński [f], Magdalena Osial [c,*]

[a] *Institute for Tropical Technology, Vietnam Academy of Science and Technology, 18 Hoang Quoc Viet, Cau Giay, Hanoi, Viet Nam*
[b] *Bydgoszcz University of Science and Technology, Faculty of Chemical Technology and Engineering, Seminaryjna 3, 85-326, Bydgoszcz, Poland*
[c] *Institute of the Fundamental Technological Research, Polish Academy of Sciences, Pawińskiego 45B Str., 02-106, Warsaw, Poland*
[d] *Faculty of Physics, University of Warsaw, Pasteura 5 Str., 02-093, Warsaw, Poland*
[e] *Centre of Radiochemistry and Nuclear Chemistry, Institute of Nuclear Chemistry and Technology, Dorodna 16 Str., 03-195, Warsaw, Poland*
[f] *Faculty of Chemistry, University of Warsaw, Pasteura 1, 02-093, Warsaw, Poland*
[g] *Faculty of Geology, University of Warsaw, Żwirki I Wigury 93, 02-089, Warsaw, Poland*
[h] *Helmholtz Centre Potsdam, GFZ German Research Centre for Geosciences, Telegrafenberg, 14471, Potsdam, Germany*
[i] *University of Science and Technology of Hanoi, Vietnam Academy of Science and Technology, 18 Hoang Quoc Viet, Cau Giay, Hanoi, Viet Nam*

ARTICLE INFO

Handling Editor: Dr P. Vincenzini

Keywords:
Drug delivery
Hydroxyapatite
Anticancer
5-fluorouracil
Curcuminoids
Nanocomposite

ABSTRACT

Nanostructural hydroxyapatite (HAp) with a uniform rod-like shapes sized in 8 ± 1 nm diameter and 45 ± 9 nm length was prepared within the facile and cost-effective co-precipitation technique as a porous platform for the immobilization and release of an anticancer drug – 5-fluorouracil. The HAp was stabilized with the biologically active curcuminoids directly extracted from *Curcuma longa* L. rhizome such as curcumin (curcumin I), demethoxycurcumin (curcumin II), bisdemethoxycurcumin (curcumin III). Due to the high surface: volume ratio HAp offered a high intake of biologically active compounds. Turbidimetry results confirmed the stability of the aqueous suspension of the modified HAp. *In vitro* tests on SKOV-3 and HepG2 model cell lines examined by MTS assay lines revealed the cytotoxicity of nanocomposite loaded with drug and curcuminoids. In addition, Langmuir trough method was used to study the effect of proposed nanocomposite on biomimetic membranes.

1. Introduction

Cancer is a plague of the 21st century and without novel solutions or early diagnostics and treatment, the battle against it might be lost. For this reason, fast development of nanotechnology brings hope in cancer's treatment. One of the solutions is based on the application of the biocompatible nanomaterials that can release anticancer drug to the affected cells, and heal the tissues [1]. They can maximize the pharmaceutical action of drugs released by reducing the toxic side effects [2]. Among many nanostructural materials, hydroxyapatite (HAp) nanoparticles reveal chemical and structural similarities with natural bone tissues, resulting in biocompatibility [3]. Therefore, it has gained attention in recent years especially in the bone diseases diagnosis and therapeutic delivery [4]. Due to its high surface-to-volume ratio and chemical composition, it promotes chemical and physical modifications making it an ideal platform for drug delivery [5–7] also having

* Corresponding author.
** Corresponding author.
E-mail addresses: ntphuong@itt.vast.vn (T.P. Nguyen), slawomir.wilczewski@pbs.edu.pl (S. Wilczewski), j.lewandows2@student.uw.edu.pl (J. Lewandowski), a.majkowska@ichtj.waw.pl (A. Majkowska-Pilip), k.zelechowska@ichtj.waw.pl (K. Żelechowska-Matysiak), dnieciecka@chem.uw.edu.pl (D. Nieciecka), waldemar.studzinski@pbs.edu.pl (W. Studziński), o.sunday@chem.uw.edu.pl (S.J. Olusegun), m.d.syczewski@gmail.com (M. Syczewski), mgiersig@ippt.pan.pl (M. Giersig), dinh-thi-mai.thanh@usth.edu.vn (T.M.T. Dinh), pakrys@chem.uw.edu.pl (P. Krysiński), mosial@ippt.pan.pl (M. Osial).

https://doi.org/10.1016/j.ceramint.2023.05.123
Received 7 January 2023; Received in revised form 11 May 2023; Accepted 13 May 2023
Available online 13 May 2023

antibicrobial activity [8,9]. As a drug carrier it can interact with biological cells resulting in multiple potentialities to be explored such as induction of apoptosis to cancerous cells, cellular proliferation, angiogenesis, or tissue recovery [10]. HAp and its composites became noteworthy choices as drug carriers in bone regeneration treatment [11,12]. The composites based on the HAp are also proposed as a platform for anticancer drug delivery [13,14] including e.g. doxorubicin [15,16], paclitaxel [17], methotreaxate [18], toceranib [19], and 5-fluorouracil [20].

It has also been recently tested in the randomized clinical trials offering high effectiveness in bone regeneration for its biocompatibility [21]. However, besides the use in the hard tissue treatment, many studies also show HAp's potential to be also used on the soft tissue. For example, Xu et al. proposed HAp as a marizomib drug carriers for the ovarian cancer treatment [22], while other work shows its use as an adjuvant in immunotherapy or as the component of multiple nanocomposites for the anticancer use [23]. Santos et al. demonstrated the HAp granules loaded with 5-fluorouracil [24], while Ji et al. [25] and Tseng et al. [26] proposed HAp nanorods loaded with the same drug as the materials for the prolonged chemotherapeutic delivery. Kundu et al. used HAp with doxorubicin for hepatocellular carcinoma defeat on *in vivo* model [27]. Another work presents HAp-based magnetic nanocomposite for HepG2 cells treatment inducing ROS [28], similarly to the work of Awwad et al. describing HAp-based composite with mesoporous magnesia for induction of the death in HepG2 cells [29]. It is seen that due to the modification of HAp or it loading with organic compounds it offers a therapeutic features in the treatment even of ovarian and liver cancers. Literature also refers HAp as a promising platform to be used in the cancer diagnostics including the use as a biomarker of liver cancer [30] or ovarian cancer [31] including even early detection of neoplasms of ovaries and other organs [32].

Generally, for to the well-developed surface of HAp, it offers effective loading of many different therapeutic compounds and their prolonged release, e.g., 5-fluorouracil release from zinc-doped HAp [33], copper bis-(8-hydroxyquinoline) released from HAp [34], or doxorubicin release from folic acid-modified HAp [35]. According to 5-fluorouracil that is one of most commonly used antimetabolites, it is widely used in the many different cancer cells including ovarian [36,37], colonorectal [38,39], pancreatic [40,41], liver [42,43], breast [44], and many other types e.g. head, neack, small intestinal, or biliary cancers [45]. As cancer cells may develop the resistance to particular type of therapy like e.g. 5-fluorouracil treatment [46], as well as the direct dosing of the drug leads to the severe toxicity [47,48], there is a deep need to propose novel formulations to improve the therapy and deliver drugs locally including the use of nanocarriers like HAp. Some studies proposed delivery of the combined agents like 5-fluorouracil with curcumin to enhance the therapeutic effect comparing to the sole drug application [49].

Curcuma longa L., also called turmeric is widely used as spice or food additive. It is also well known in a traditional medicine in Asia [50]. This plant contain many valuable chemical compounds revealing biological activity, where the main active compounds are curcuminoids including curcumin I (known as curcumin), curcumin II (known as demethoxycurcumin), and curcumin III (known as bisdemethoxycurcumin), monoterpenoids, and sesquiterpenoids [51,52]. For the rich curcuminoids content, the turmeric extract is widely referred with literature for anti-inflammatory, anti-oxidative and anti-cancer activity [53,54]. *Curcuma longa* L. offers promising anticancer effectiveness against different cancer types with very low or negligible toxicity to healthy cells. It is also presented it has curcuminoids reveal alleviating and suppressing the generation, transformation, proliferation, and metastasis of many different types of cancer cells [55]. Additionally nanoparticle-mediated delivery of curcumin can improve the pharmacokinetic profile of medicines raising the chemotherapeutic potential [56]. Curcuminoids bring a lot of attention in anticancer research for their biological activity. For example, turmerones being active ingredients in turmeric oil, has mainly anti-cancer property [57]. Therefore, both curcuminoids and other components of *Curcuma longa* L. rhizome account for the pharmacological efficacy of turmeric [58].

This work demonstrates the nanocomposite that brings together the nanosized hydroxyapatite loaded with the anticancer drug, in particular 5-fluorouracil and the curcuminoids. HAp offers non-cytotoxicity and well-developed surface so it can be effectively loaded with different compounds. The curcumin extract obtained from the *Curcuma longa* L. rhizome was proposed as a source of the biologically active components with high-efficiency and low-costs of preparation. As the freshly prepared extract contains more active ingredients comparing to the commercially available curcumin powder, its composition was confirmed with High Pressure Liquid Chromatography (HPLC) and gas chromatography (GC). The compounds from the extract improved the stability of the colloidal suspension and the cytotoxicity of the 5-fluorouracil towards the SKOV-3 and HepG2 cells. Both type of cells are widely used as an ideal solid human cancer model for anticancer therapeutic and diagnostics [28–32]. Therefore, these cell lines were chosen to test the effect of HAp@cur@5-flu nanocomposite as an anticancer drug platform. The results demonstrate the proposed nanocomposite as a promising material interacting with biomimetic membranes and defeating cancer cells.

2. Experimental

2.1. Materials

The $Ca(NO_3)_2$ calcium nitrate (V), $(NH_4)H_2PO_4$ ammonium dihydrogenphosphate and 25% NH_3 ammonia solution with the analytical grade were purchased from POCH, Poland. Deionized water with resistivity 18.2 MΩ cm at 25 °C was obtained using the Milli-Q ultra-pure water filtering system (Merck, Darmstadt, Germany). The *Curcuma longa* L. rhizome extract obtained as in our earlier work [59]. NaCl with analytical grade was purchased from Warchem, Poland. The 5-fluorouracil ≥99% grade was purchased from Sigma-Aldrich, Germany.

The following materials were used for cell experiments: McCoy's Medium, Eagle's minimal essential medium (EMEM), trypsin-EDTA, phosphate-buffered saline (PBS), fetal bovine serum, L-Glutamine, a penicillin/streptomycin solutions from Biological Industries (Biological Industries, Beth Haemek, Israel), and dimethyl sulfoxide (DMSO) (Sigma-Aldrich, St. Louis, MO, USA), CellTiter 96® Aqueous One Solution Reagent (MTS compound) from Promega (Promega, Madison, WI, USA).

A human-derived SKOV-3 cancer cell line was obtained from the American Type Culture Collection (ATCC, Rockville, MD, USA). It was cultured in McCoy's medium supplemented with 10% fetal bovine serum and 1% penicillin/streptomycin, where the cells were cultivated at 37 °C in a humidified atmosphere containing 5% CO_2. The HepG2 cell line was cultured similarly, while 1% L-glutamine was used in addition.

Langmuir monolayers were prepared with a KSV-Nima KN2003 trough system with the KSV NIMA LB Software (Biolin Scientific, Manchester, UK).

2.2. Synthesis of the hydroxyapatite

Hydroxyapatite (HAp) nanoparticles were prepared by co-precipitation within the procedure described as follows: 0.59 g of $Ca(NO_3)_2$ (calcium nitrate (V)) was placed into a beaker and dissolved in 5 mL of deionized water. The solution containing 0.33 g of $(NH_4)_2HPO_4$ diammonium hydrogen phosphate that was dissolved in the 5 mL of water, was put in the burette above the beaker that contained the solution of $Ca(NO_3)_2$. Also placed above the beaker is the another burette that was filled with 25% ammonia solution.

To precipitate the HAp both solutions from the burettes were added dropwise to the beaker, where the ammonia water was used as a precipitating agent. The pH during precipitation was adjusted to 11. After phosphates and ammonia addition, the suspension was stirred

continuously for 4 h. Then, HAp suspension was washed with distilled water and centrifuged at 3500 rpm for 10 min. Washing of HAp was performed several times until reaching neutral pH.

2.3. Modification of the hydroxyapatite

The 30 mg of curcumin extract was added into the 10 mL of aqueous suspension containing 100 mg of HAp and 30 mL of methanol was added to dissolve the extract. The suspension was continuously stirred with 500 rpm for 1 h, then placed into the Falcon tube, and centrifuged at about 2000 rpm for 5 min. Then, the supernatant was removed and replaced with water. The suspension was shaken for 2 min and sonicated for 5 min. After sonication the suspension was centrifuged to remove excess curcumin extract and the procedure was repeated three times.

The next step was loading of the 5-fluorouracil to curcuminoids-modified nanohydroxyapatite (HAp@cur), where the 15 mg of drug was placed in the colloidal suspension and HAp@cur and stirred overnight with 300 rpm at room temperature. Then, the suspension was centrifuged at about 2000 rpm for 5 min, washed with Milli-Q water, and centrifuged again. Finally, the suspension was suspended in 30 mL of water, where the suspension was shaken on a vortex for 3 min. The final result was a nanohydroxyapatite nanocomposite with loaded extract and 5-fluorouracil (HAp@cur@5-flu).

2.4. Methods

The extraction of turmeric was performed using B-811 Büchi Soxlet extractor (Switzerland). Curcuminoid analysis was performed using a Shimadzu UFLCXR liquid chromatograph with a detector with SPD-M30A photodiode array. UV–Vis spectra were acquired from 200 to 800 nm. A Phenomenex Luna 3u C18 (2) 100 A (150 × 3.0 mm) column was used for HPLC analysis. Column temperature was set to 48 °C. The gradient elution profile was as follows: (A) water (0.25% HOAc) and (B) acetonitrile, 0–17 min, 40–60% B, 17–28 min, 60–100% B; 28–35 min, 100% B; 35–40 min, 100–40% B at a flow rate of 0.8 mL min^{-1}.

Compounds adsorbed on HAp was also tested on an Agilent 7890 B GC System gas chromatograph with an Agilent 5977 B GC/MSD mass spectrometry detector. An HP-5MS column (0.25 mm × 30 m x 0.25 μm) was used for the tests. The analyzes were performed under the following chromatographic conditions: injector temperature 250 °C, detector temperature 280 °C, oven temperature program from 50 °C/4 min - increase of 15 °C min to 300 °C (maintained for 10 min). Helium was used as a carrier gas, gas flow was set at 1 $mlmin^{-1}$. The volume of the dosed sample was 1 μL. The substances were identified by comparing the obtained MS spectra with the spectra of the NIST17. L Mass Spectrum Library.

The morphology studies were performed by the Scanning Electron Microscopy (SEM) — Merlin, ZEISS, Stuttgart, Germany and Transmission Electron Microscopy (TEM) — Zeiss Libra 120 Plus, Stuttgart, Germany, operating at 120 kV. Hydrodynamic diameter and the zeta potential of the particles were measured with a Malvern Zetasizer instrument (Nano ZS, UK) fitted with He–Ne laser (λ = 632.8 nm) as the light source at the scattering angle of 173°, where the ionic strength was adjusted with NaCl to 0.01 M in case of the surface potential determination.

The X-ray diffraction analyses (XRD) were performed using the DSH method on a Malvern Panalytical X'Pert PRO MPD powder diffractometer. The XRD patterns were recorded in the (2θ) range from 18° to 85°, with a scan rate of 1° per minute with total record time of 67 min. Analysis were done with using Co Kα at 40 kV and 40 mA. Phase identification was obtained with the use of X'Pert Plus HighScore software with access to the COD (Crystallography Open Database) database. The crystallite sizes were calculated using a Scherrer formula.

The specific surface area of HAp sample was determined based on the low-temperature nitrogen adsorption isotherms following the Brunauer, Emmett, and Teller (BET) method, using a Micrometrics ASAP 2000 instrument.

The characterization of HAp, HAp@cur, HAp@cur@5-flu was carried out by Fourier-transform infrared spectroscopy (FT-IR) using the ATR technique (Alpha apparatus) supplied from Bruker. The measurements were performed in the range of 4000–400 cm^{-1}, where the 32 scans at a resolution of 4 cm^{-1} were performed.

The amount of deposited components in the nanocomposite was assessed by the thermogravimetric method (TGA) using a TG 209 F3 Tarsus apparatus (Netzsch). The heating rate was about 10 °Cmin^{-1} in an open ceramic crucible under nitrogen atmosphere, in the temperature range from 30 to 700 °C.

The stability water suspension of the obtained composite was carried out using the multiple light scattering method by Turbiscan Lab apparatus (Formulaction SA, France), where the colloidal suspension of HAp in water was placed in glass cylindrical measurement test tubes with a working height of 54 mm. Then, the samples were placed in a Turbiscan Lab apparatus (Formulaction SA, France) and subjected to scanning with light at a wavelength of about 880 nm. The scans were carried out every 3 min for half an hour at room temperature (23 °C). Based on the obtained results, the Turbiscan Stability Index (TSI) was determined.

The Langmuir test was carried out in the following stages, trough and barriers were cleaned with chloroform and methanol to remove potential impurities before each measurement. Wilhelmy's platinum plate was flamed to remove all contaminants from the surface. The trough was filled with the subphase solution (Milli-Q water or solution of drug/carriers), and then, 30–40 μL of a chloroform solution of the selected lipid at a concentration of 2 mg mL^{-1} was dropped. After about 15 min, when the solvent had evaporated, the layer was compressed. The experiments were carried out with a 5 cm^2 min^{-1} barrier movement speed until the surface pressure reached the value 30 mN m^{-1}.

In Cytotoxicity studies prior to the cells treatment with the proposed nanocomposite and particular ingredients of the composite, the cells (2.5×10^3 SKOV-3, 10×10^3 HepG2) were seeded in 96-well plates and incubated under 5% CO_2 atmosphere at 37 °C. Then, the medium was removed, compounds were added and incubated for 24 h and 48 h. After a suitable time, the medium with compounds was removed, the wells with cells were washed with PBS and fresh medium and MTS reagent were added. After 2 h of incubation, the absorbance was measured at 490 nm and the cell viability was evaluated.

To analyze the experimental data, GraphPad Prism version 8.0 software (GraphPad Software Inc., San Diego, CA, USA) was applied. Values between groups were compared using one-way ANOVA. The results are presented as mean ± standard error of the mean (SEM) and were considered as statistically significant when $p \leq 0.05$, $p \leq 0.01$, $p \leq 0.001$, and $p \leq 0.0001$.

3. Results and discussion

3.1. Characterization of extract compounds adsorbed on HAp

Prior to the loading of the obtained curcumine extract into the HAp nanostrcutres, the biologically active compounds were identified with the high-pressure liquid chromatography. From the HPLC analysis, it can be concluded that the three major curcuminoids (curcumin, demethoxycurcumin and bisdemethoxycurcumin) are sorbed on the hydroxyapatite (Fig. 1a). On the basis of comparison with reference materials, bisdemetoxycurcumin (1) with a retention time of tR = 6.154 min, demethoxycurcumin (2) with a t_R = 6.764 min, and curcumin (3) with a t_R = 7.404 min were identified. Based on the GC-MS analysis (Fig. 1b), it was found that also the following compounds are sorbed *ar*-curcumene (4), (−)-zingiberene (5), b-zesquiphelandrene (6), b-turmerone (7), (6R, 7R)-bisabolene (8), (E)-atlantone (9). All of these compounds reveal biological activity [60–63]. Table 1 shows the selected *m/z* signals of the identified compounds marked on chromatograms as 1–9. The presence of these compounds in the extract offer the broad spectrum of the biomedical application including

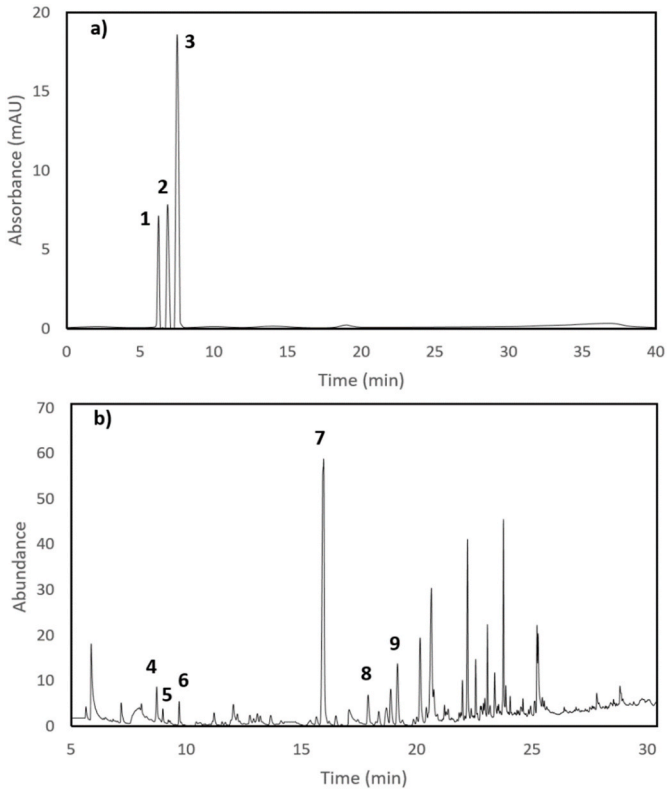

Fig. 1. Chromatograms of turmeric extract sorbed on hydroxyapatite: a) HPLC analysis, b) GC-MS analysis.

Table 1
List of compounds with selected *m/z* signals.

Signal	t_R, min	Name of compound	Selected *m/z* signals (% of base peak)
4	8.712	*ar*-Curcumene	105 (56), 119 (100), 132 (74), 202 (24)
5	8.973	(−)-zingiberene	69 (40), 93 (100), 119 (94), 204 (10)
6	9.685	b-sesquiphelandrene	69 (100), 93 (50), 133 (20), 161(20), 204 (10)
7	15.949	b-turmerone	55 (20), 83(40), 105 (19), 120 (100), 218 (5)
8	17.879	(6R,7R)-bisabolene	95 (45), 110 (58), 137 (100), 204 (10)
9	19.16	(E)-atlantone	83 (100), 123 (35), 135 (42), 203 (20), 218 (10)

anti-inflammatory, antioxidative, and anticancer effects [64–67].

Comparing the composition of compounds in the crude turmeric extract that is presented in our previous work [32] it is seen that from the 11 biologically active compounds only *ar*-turmerone (10) and a-turmerone (11) were not sorbed on the HAp. Both the composition of sorbed substances on hydroxyapatite and turmeric extract is similar to the compounds identified by Li [68] and Xu [69].

3.2. Morphology studies

The morphology of prepared composites was studied with Scanning Electron Microscope (SEM) and Transmission Electron Microscope (TEM). SEM images are presented in Fig. 2 in the left column, while TEM images are presented in the right column. As can be seen in Fig. 2a bare HAp shows agglomeration of nanoparticles of irregular shape and spiky structures, while TEM images (Fig. 2b) reveal needle-like agglomerates. Subsequent Fig. 2c and d reveal the HAp modified with curcuminoids. SEM image shows similar morphology full of bulky clusters. However, TEM analysis confirms the needle-like structure of the HAp similarly to the structures described in literature [70,71]. The morphology of HAp modified with organic compounds is similar to the results presented in the literature [72]. After the loading of the 5-fluorouracil into the HAp@cur structures the composite looks similar to those after the initial modification with curcuminoids. As can be seen in Fig. 2 e-f the needle like structures are also revealed that occur within the whole sample, where the average diameter of a rod is about a few nm and even a 70 nm in length.

3.3. Hydrodynamic size, crystallinity of HAp, and adsorption capacity

Complementary to the TEM analysis, DLS studies have shown the hydrodynamic size of the composite loaded with drug of about 70 nm Fig. 3a. Then, the surface charge was determined, where the bare HAp has −9.4 mV surface potential, while it tends to aggregate similarly to the results described in the literature [73]. The measurements were performed in the PBS solution. The zeta potential for the HAp loaded with curcuminoids was about 7.3 mV indicating that the particles were positively charged what improves the loading of the 5-fluorouracil into the HAp.

The structure of prepared HAp was investigated with XRD technique based on recorded patterns. Fig. 3b confirms the presence of reflections peaks at 20.07, 24.91, 27.23, 32.03, 33.68, 40.20, 43.66, 45.16, 48,92, 52.55, 57.63, 60.04, and 66.89° corresponding to its main diffraction planes: (200), (002), (207), (211), (300), (310), (311), (203), (222), (104), (322), (420), and (304), being in the good comparison to the results presented in the literature [74–77]. The HAp presence in the sample was also identified based on the 96-901-1092 card from the Crystallography Open Database (COD). The size of crystallites is ranging around a few dozens of nanometers, which is also confirmed by electron microscopy studies.

The size of the crystallites D was estimated using the Scherrer formula, equation (2) [78]:

$$D = \lambda K(\beta(\cos\theta))^{-1} \quad (2)$$

Where the β stands for the full width-at-half-maximum length of the reflection, θ is the Bragg angle, λ is the X-ray wavelength, and K is a dimensionless shape factor (0.94).

So far, the crystallites size D is about 29.21 ± 2.86 nm what in the good agreement with the TEM studies referring to the diameter of the obtained samples.

The specific surface area of hydroxyapatite structures was determined by the Brunauer-Emmett-Teller (BET) method, using nitrogen adsorption at 77 K. Fig. 4 shows the characteristic N_2 adsorption/desorption isotherm revealing a typical type IV isotherm curve with a hysteresis loop. It points out the presence of mesopores [79,80] where the average size of pores is 14.54 nm. The material shows the specific surface about 105.02 ± 0.76 $m^2\ g^{-1}$ confirming the high adsorption capacity making it possible to load curcumin extract and the drug for further *in vitro* studies. This BET specific surface area obtained in this study is higher than 32 $m^2\ g^{-1}$ that had been earlier reported for HAp in another study [81]. Isotherm obtained from the partial pressure is presented in the inset.

3.4. Chemical composition and content of organic compounds

The FTIR spectra of HAp, HAp@cur, and HAp@cur@5-flu can be seen in Fig. 5a the peaks in the range 500–600 cm^{-1} can be ascribed to PO_4^{2-} groups. The following bands at 1000–1200 cm^{-1} are also characteristic to these groups [82–84]. The 1620 cm^{-1} band comes from the bending vibration of water, while the intralayer H-bonded and also O–H stretching can be ascribed to the broadband centered at 3400 cm^{-1} [85,86]. The bands at 2920 cm^{-1} and 2850 cm^{-1} are the presence of C–H vibration [87] and 1581 cm^{-1} is characteristic to the C═C aromatic stretching [88,89]from the organic compounds coating HAp. It is in a good agreement with the peaks that are present in the bare curcumin

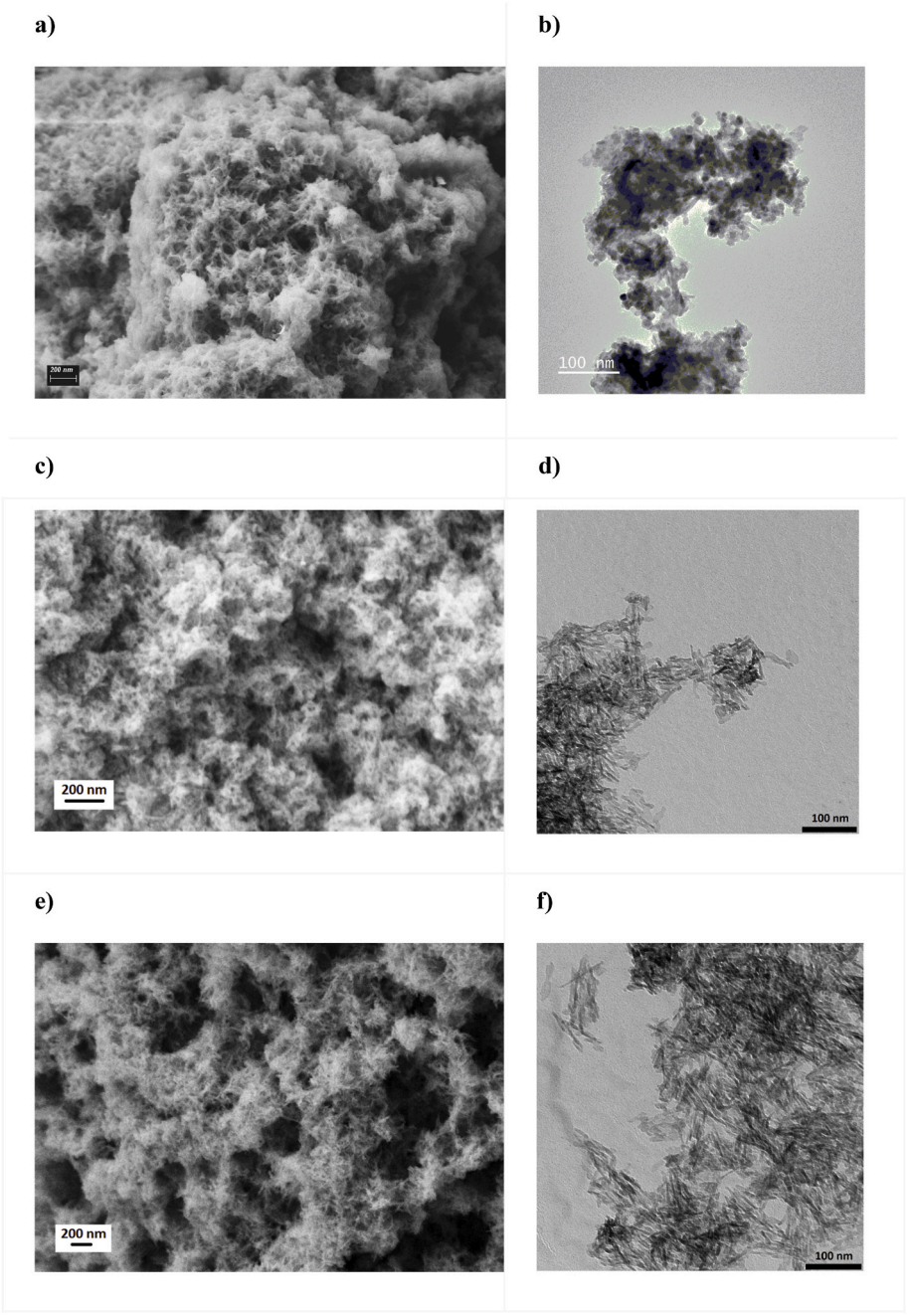

Fig. 2. a) SEM and b) TEM images of HAp, c) SEM, d) TEM images for HAp@cur composite, and e) SEM, f) TEM images of HAp@cur@5-flu

extract and the 5-fluorouracil samples, see inset in Fig. 5a. Due to the presence of 5-flu the following bands can be ascribed: 1725 cm^{-1} for the cyclic imide, CONHCO, 1672 cm^{-1} for imide, amide II band (C═O), and 1247 cm^{-1} for amide III band (C–O) [90–92]. Based on the recorded spectra, it is seen that the coating of HAp with curcuminoids leads to the increase the number of hydrogen bond interactions. The narrow band for stretching of O–H group at about 3520 cm^{-1} is not seen and the intensity of the bands in the range from ~1300 to 1500 cm^{-1} is increased in the presence of curcuminoids in the HAp@cur. For the HAp@cur@5-flu the same interactions appear between the HAp and the drug as well between both organic compounds, so the intensity of the bands in range mentioned above also is raised. Additionally, due to the presence of double bonds in the both molecules, the π-π interactions between curcuminoids and 5-fluorouracil can also be assumed.

The thermogravimetric analysis (TGA) (Fig. 5b) was performed to estimate the content of organic compounds in the HAp matrix. Gradual mass loss is observed in the thermogram of HAp from 30 °C to 200 °C which is due to loss of bound water. The increase in temperature after 200 °C did not insignificantly lead to loss of mass. This implies that HAp is relatively thermally stable at the temperature above 200 °C.

In the case of HAp@cur and HAp@cur@5-flu the presence of organic molecules (Curcumin extract and 5-fluorouracil), led to a significant mass loss when the temperature was above 200 °C. The observed mass loss was due to the decomposition of both Curcumin extract and 5-fluorouracil that were loaded in the HAp matrix. As can be seen in thermogram the content of Curcumin extract is about 14%, while after the 5-fluorouracil loading, the additional decrease about 2% due to the decomposition of drug was observed [93–95]. Therefore, it is assumed that HAp@cur@5-flu is loaded with 14 μM of curcuminoids and 2 μM of 5-fluorouracil per 100 μM of HAp. The FT-IR analysis and TGA results

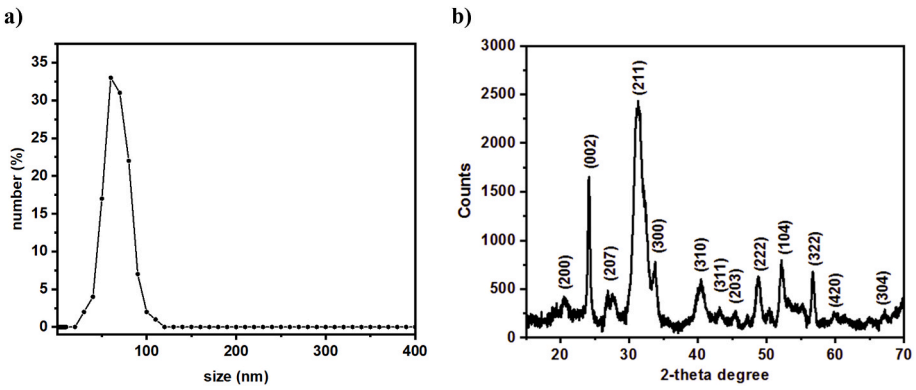

Fig. 3. a) distribution of hydrodynamic diameter and b) XRD pattern for HAp (vs. Cu cathode).

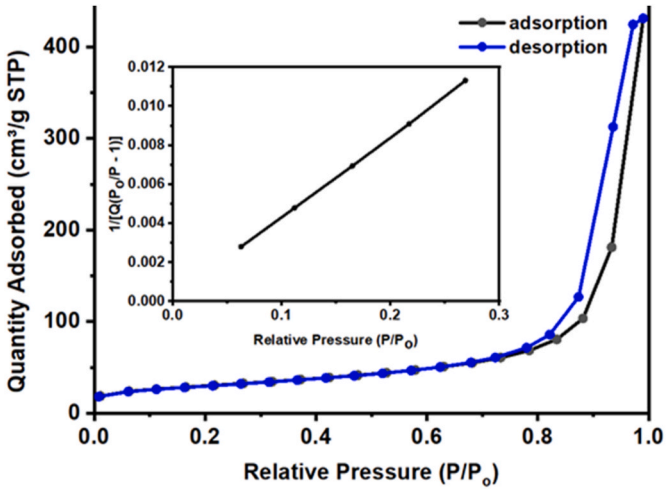

Fig. 4. The N_2 adsorption isotherm for the HAp.

confirmed the presence of both, curcuminoids and the drug in the nanocomposite.

3.5. Turbiscan analysis

The stability of the nanocomposite-based suspension was investigated with the multiple light scattering method, namely turbiscan method. It makes it possible to determine the flocculation, aggregation, or sedimentation of tested material etc. [96–98]. The sample plots presented in Fig. 6 show percentages of transmitted light (LT) and backscattered light (BS) over the 1.5 mg mL^{-1} vs. height of the sample for HAp suspension in distilled water. Based on the turbiscan analysis it is seen that the prepared suspension was stable (T = 0%) at initial observations., while the transparency increase Fig. 6a, over time was observed at the top of the sample indicating partial sedimentation of the nanocomposite-based suspension [99,100]. This is confirmed by the densification of the lower suspension layer, over time which is manifested by an increase in the BS intensity, in the lower part of the sample, see Fig. 6b. Suspensions of both HAp@cur and HAp@cur@5-flu nanocomposites underwent the same destabilization mechanism.

On the basis of the obtained results of the stability of nanocomposite suspensions, the destabilization kinetics of the prepared systems was determined (see Fig. 7). For this purpose, the Turbiscan Stability Index (TSI) was determined with the help of software supplied by the manufacturer. The TSI is the most efficient method of quantitative comparison of several regions in the sample between each other. The higher the TSI, the more unstable the system is 45.50. Due to the sedimentation, the TSI was determined in the upper part of the sample (H = 36–54 mm), where the changes in the stability of the systems were most noticeable, see Fig. 6a. On the basis of these results, it was found that HAp@cur, HAp@cur@5-flu form stable suspensions in water. The use of the *Curcuma longa* L. rhizome extract improved the HAp stability as well as the 5-fluorouracil loading for the presence of many functional groups, what is required to be used in the following *in vitro* studies.

3.6. Influence on biomimetic Langmuir films

Following studies were performed to evaluate the influence of various substances on the biomimetic monolayers formed on the

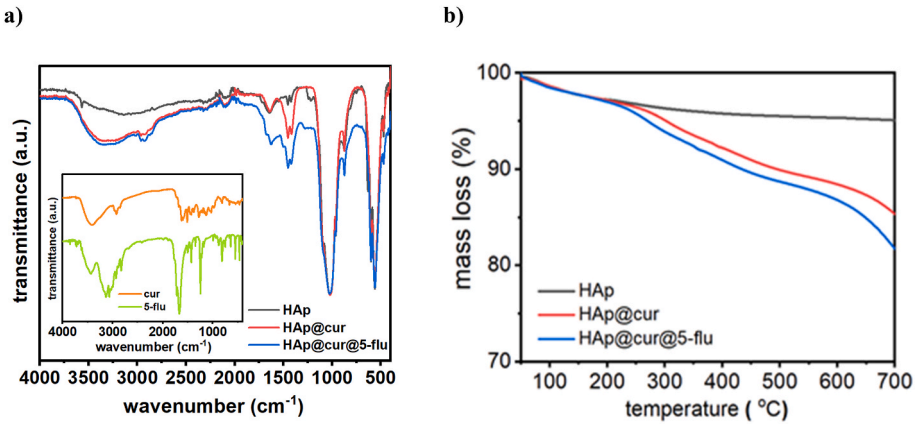

Fig. 5. a) FT-IR spectrum for HAp, HAp@cur, and HAp@cur@5-flu (inset presents spectra for bare cur and 5-flu) and b) TGA curves of HAp, HAp@cur, and HAp@cur@5-flu.

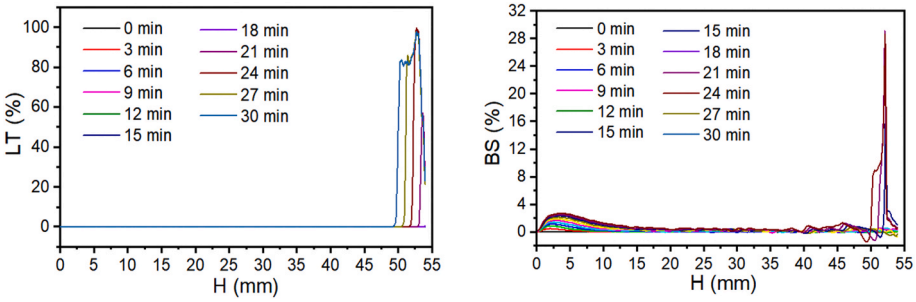

Fig. 6. a) percentages of transmitted light over the height of the sample, b) percentage of backscattered light over the height of the HAp.

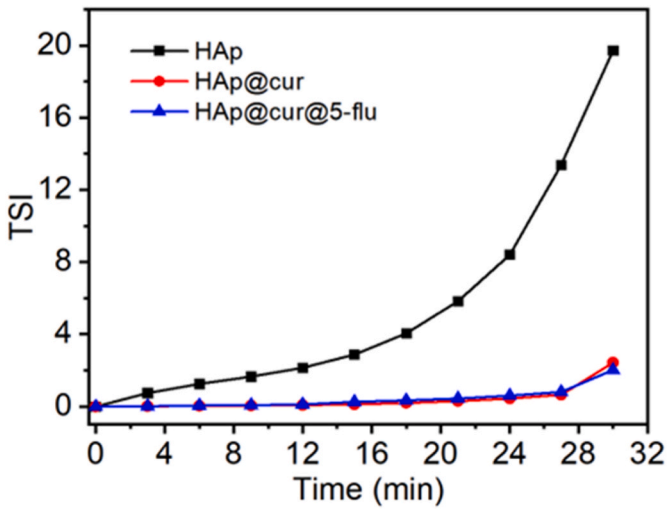

Fig. 7. Turbiscan Stability Index change in time.

Langmuir trough being analogs of biological membranes [101,102]. The Langmuir technique enables the formation of such analogs with respect to their composition and organization to the natural membranes making it possible to test their interactions with drugs and drug carriers [103]. Cell membranes, depending on their functions, consist of a mixture of lipids with different structures and acid-base properties. Therefore, in the described research for creating Langmuir monolayers, we used 3 different types of lipids: DOPC (1,2-dioleoyl-*sn*-glycero-3-phosphocholine), DOPE (1,2-dioleoyl-*sn*-glycero-3-phosphoethanolamine) and cardiolipin to mimic cancer cells like SKOV-3 and HepG2 cell lines. Phosphatidylcholine is a neutral lipid and it is the most abundant compound of the lipid bilayer also in the cancer cell. DOPC is mostly present in the outer leaflet of the plasma membrane which is important because the drug or conjugate, penetrating inside the cell, first interacts with the outer part of the cell membrane. Phosphatidylethanolamine is the second most common membrane phospholipid with basic properties because of the amine group in their structure. Phosphatidylethanolamine is present on both sides of the plasma membrane however in many cancer cell types, PE distribution is reversed with a greater preference for the outer leaflet of the cell membrane. The last selected lipid was cardiolipin, a compound with acidic properties. There are hypotheses that cancer cells can modify the content and composition of cardiolipin in cells, influence cardiolipin metabolism, and change the properties of the membrane.

The subphases in these studies were as follows: Milli-Q water, 5-fluorouracil solution (5-flu), hydroxyapatite suspension (HAp), suspension of HAp loaded with curcuminoids (HAp@cur) and hydroxyapatite suspension modified with curcuminoids and anticancer drug (HAp@cur@5-flu). Comparative isotherms have not been recorded for pure curcumin extract due to partially hydrophobic properties. In the beginning, the influence of HAp on the resulting biomimetic layers was investigated (blue curves in each graph – Fig. 8). Two concentrations of hydroxyapatite, 4.5 mg mL^{-1}, and 10 mg mL^{-1}, determined as C1 and C2, were used in the studies. Plots of the surface pressure (π) as a function of surface area (A) for a single lipid molecule, called π-A isotherms are shown in Fig. 8.

Fig. 8a shows the recorded isotherms for DOPC lipids. It turns out that the addition of only a small amount of pure hydroxyapatite (C1) causes the curve to shift by about 23% in relation to the milli Q subphase. The use of a higher concentration of the carrier does not affect the lipid organization so significantly, which may indicate that the carrier accumulates in the lipid layer only in a specific concentration range. The explanation of this phenomenon may also be related to the different organization of the lipid (different angle of the lipid molecule on the surface of the subphase) in the presence of high concentrations of HAp. The modification of the nanocarrier with curcumin causes a significantly lower increase in the surface area/particle compared to the subphase with pure carriers. The addition of a lower concentration of modified hydroxyapatite increases the surface area only by approx. 7% compared to the Milli-Q water subphase. These values are similar for both concentrations of the carrier with curcumin (data not shown). It is noticeable that the addition of curcumin reduces the interaction between the lipid and the components of the subphase and affects the way of accumulation of the carrier in the lipid structure. These changes in the course of isotherms may also be related to the higher stability of the nanosystem after modification with curcuminoids.

In the next stage, the influence of modification with 5-fluorouracil and curcumin hydroxyapatite on the formed biomimetic layers was studied. The addition of fluorouracil to the subphase causes an accumulation of the drug in the area of hydrophilic lipid heads (about 10%), which is expressed by increasing the surface area per DOPC molecule. Changing the concentration of the drug has no influence on this effect, the isotherms for both concentrations (10^{-7} M and 10^{-6} M) converge (data not shown). It turns out that the modification of hydroxyapatite by drug contributes to different adsorption in the layer of 5-fluorouracil, there is a slight isotherm shift (about 7%) in relation to the subphase with a pure anticancer drug. The drug is incorporated into the interior of the carrier by the adsorption process in the pores of hydroxyapatite. The functional groups of the therapeutic are not blocked by a chemical bond however, some of them may be hidden within the carrier structure and thus it may have an influence on the interaction with the membrane. Additionally, the presence of fluorouracil influences the different slopes of Langmuir isotherms, which suggests greater fluidity of the membrane in the presence of the therapeutic (red and magenta curve in Fig. 8a).

The second lipid used in the research was DOPE, the Π-A curves obtained as a result of compression of the DOPE lipid monolayer are presented in Fig. 8b. The influence of pure hydroxyapatite on the structure of the DOPE membrane is related to the adsorption of nanostructures in the area of the hydrophilic part of the film. However, the isotherms recorded for different concentrations of the pure carrier and its forms with curcumin show slight shifts in the graphs (data shown for selected concentration). It can be concluded that for this effect, the

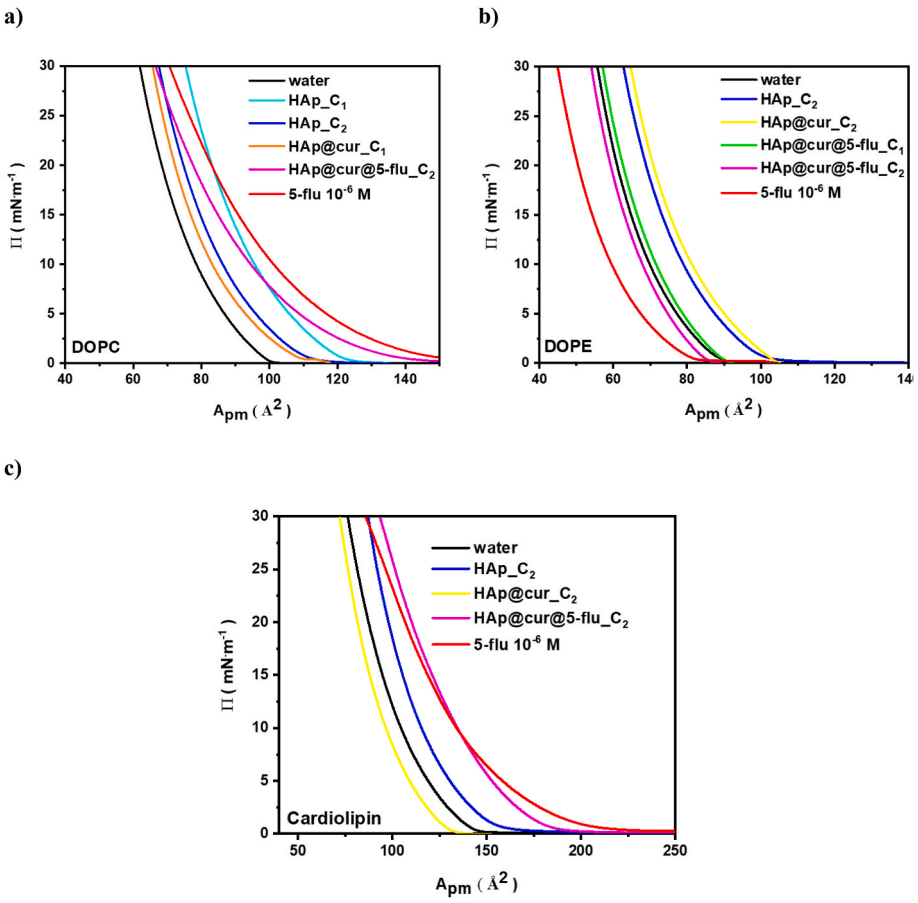

Fig. 8. Langmuir isotherm for lipids: DOPC (a), DOPE (b), and cardiolipin (c); composition of the subphase marked on the graphs.

concentration of the carrier and the contact time with the membrane are irrelevant. 5-Fluorouracil strongly interacts with the membrane. On the isotherm, it is visible as a shift of the curve to the left, which may be related to a different angle of the lipid position in relation to the water subphase.

The presence of a drug concentration of 10^{-6} M in the subphase decreases the surface area by about 18%. Too strong accumulation in the membrane is not a favorable phenomenon because it may limit the penetration of the therapeutic into the cell. The use of a fluorouracil carrier may contribute to weaker adsorption of the compound that will be locked inside the nanostructure. Based on the recorded isotherms, it can be seen that the incorporation of the drug inside the hydroxyapatite structure results in a lower accumulation of such conjugate in the membrane DOPE (characterized by the presence of amino groups).

The binding of the drug to the carrier reduces its affinity for the polar part of the lipid layer, as the surface area increases in relation to the free drug.

The last of the examined lipids was cardiolipin - a lipid with acidic properties of the polar head (Fig. 8c). The content of a small concentration of hydroxyapatite in the subphase causes an increase in the surface area per molecule by about 15%, but there is no correlation with the concentration of hydroxyapatite. The adsorption of curcumin in hydroxyapatite contributes to a significant reduction of the surface area in the isotherm (by approx. 13% in the case of a lower concentration of the modified carrier and by approx. 17% in the case of a higher concentration of the modified carrier). Probably, curcumin, by changing the surface properties of the carrier, contributes to the reduction of penetration of nanostructures into the membrane, the same as in most of the tested layers.

Fluorouracil in the range of high concentrations (10^{-6} M) accumulates in the cardiolipin layer not so strong as anthracycline [104]. The encapsulation of the fluorouracil in hydroxyapatite does not reduce the way of adsorption of the compound in the region of the hydrophilic polar groups of the lipid compared to the free drug. Modification of the carrier with a therapeutic agent causes visible changes in the slope of the isotherm, which suggests a change in the fluidity of the layer (red and magenta curves).

The surface pressure – area per molecule measurements allowed estimation the effect of hydroxyapatite and its conjugates on the structure of monolayers formed by the selected phospholipids. The results of those studies showed the degree of incorporation of the drugs or compounds and their conjugates into the layers and changes in the properties of the monolayers upon compression in the presence of the nanosystem.

The results have shown the ability of modified hydroxyapatite to interact with and/or to insert among phospholipid molecules in membrane especially in the presence of choline. In this case, even a small addition of a pure carrier significantly influences the isotherm shift. The presence of curcumin changes the surface properties of the conjugate, which contributes to the low affinity of the nanocarrier to most of the tested membranes. The obtained results suggest that fluorouracil has a strong affinity for the lipid However, drug adsorption in hydroxyapatite significantly reduces this type of drug-lipid interaction. For most of the tested lipids, the addition of the conjugate changes the fluidity of the membrane and can alter functional properties of membrane. Moreover, pathological processes in living cell can also be related to fluidity modifications.

The effect of drugs nanocarriers on the structure of cell membranes is an important part of the overall effectiveness of conjugates. These effects can be studied systematically using model membrane systems. Langmuir monolayer provide the advantage of a system with reduced complexity and control over the individual constituents. While model membranes

will never be able to entirely replace *in vitro* studies, they can provide a useful first screening platform for the investigation of nano-system–membrane interactions. Therefore, the following studies included *in vitro* tests.

3.7. In vitro cytotoxicity results

Following, the cytotoxicity studies with the use of MTS colorimetric assay were performed, where the composite and bare components were tested. SKOV-3 cells were chosen to test proposed nanocomposite based on the literature findings, where the HAp was used as an anticancer drug delivery platform as well as the biomarker for ovarian cancer imaging [22,31,32,36]. According to the HepG2 cells, it was chosen to compare the therapeutic effect on the cell line that has a different susceptibility on the oxidative stress than the first cell line [27–29]. To determine cytotoxic effect on cells, they were incubated with various concentrations (50, 100, 200 μM) of HAp, curcuminoids, 5-flu, HAp@cur, and @HAp@cur@5-flu for 24 h and 48 h. The viability of the control group of SKOV-3 and HepG2 was set to 100%. As can be seen in Fig. 9 the hydroxyapatite was not toxic up to 100 μM, similarly to the literature [105], whereas higher concentration (200 μM) decreased the viability to ~85%. It can be caused by the agglomeration of the HAp onto the cells [106]. Several literature studies indicate the correlation between the size and shape of HAp and its cytotoxicity [107,108]. For example Huang et al. present that the cytotoxicity of HAp is affected by various physical parameters, electrical conductivity, surface potential, and specific surface area [68]. The addition of free curcumin to cells, did not cause any cytotoxicity even at very high concentration 200 μM. Interestingly, bound curcumin to HAp decreased slightly the viability, but only of SKOV-3 cells at high concentrations. It can also be noticed that 5-fluorouracil and HAp@cur@5-flu cytotoxicity increased in time and concentration dependent manner. In the case of ovarian cancer cells, which were treated with 5-fluorouracil attached to HAp@cur, the viability was higher than for cells treated with only free chemotherapeutic. It is in agreement with our previous studies where other cytostatic drug – doxorubicin bound to SPION@CA nanoparticles was used [77]. On the contrary, these results were not similar for HepG2 cells, where after 24 h and 48 h of incubation, the cytotoxicity of 5-flu was lower than HAp@cur@5-flu. The results clearly indicate that nanocomposite loaded with curcumin extract and anticancer drug to HAp@cur@5-flu exhibits cytotoxicity for SKOV-3 and HepG2 cancer cells. Synergistic effect curcumin and 5-fluorouracil was also demonstrated for HT-29 colon cancer cell line [109–111] and hepatocarcinoma cell line [112].

As mentioned before, based on the TGA measurements, the amount of adsorbed drug and curcumin was estimated at 2 μM and 14 μM respectively per 100 μM of HAp. The values of half-maximum inhibitory concentration (IC50) that is a measure of drug's efficacy are presented in Table 2. As can be seen the highest efficacy is observed for the drug-loaded nanocomposite on HepG2, where 42.45 μg mL^{-1} in 24 h and 20.67 μg mL^{-1} in 48 h is determined. This effect can be related with the specific antioxidative properties of the nanocomposite on the HepG2 cell line that has a relatively high hypoxia effect [113]. The IC50 values are in the good agreement with the work presenting 5-Fluorouracil (5-flu) and curcumin (CUR) loaded chitosan/reduced graphene oxide (CS/rGO) nanocomposite effect on HT-29 cells, where IC50 is 23.80 μg mL^{-1} in 48 h [114]. Other work also shows the change of the therapeutic profile of the drug on different cell lines depending on the modification of the composition of delivered molecules [115].

The release of the drug into SKOV-3 and HepG2 cell lines could occur

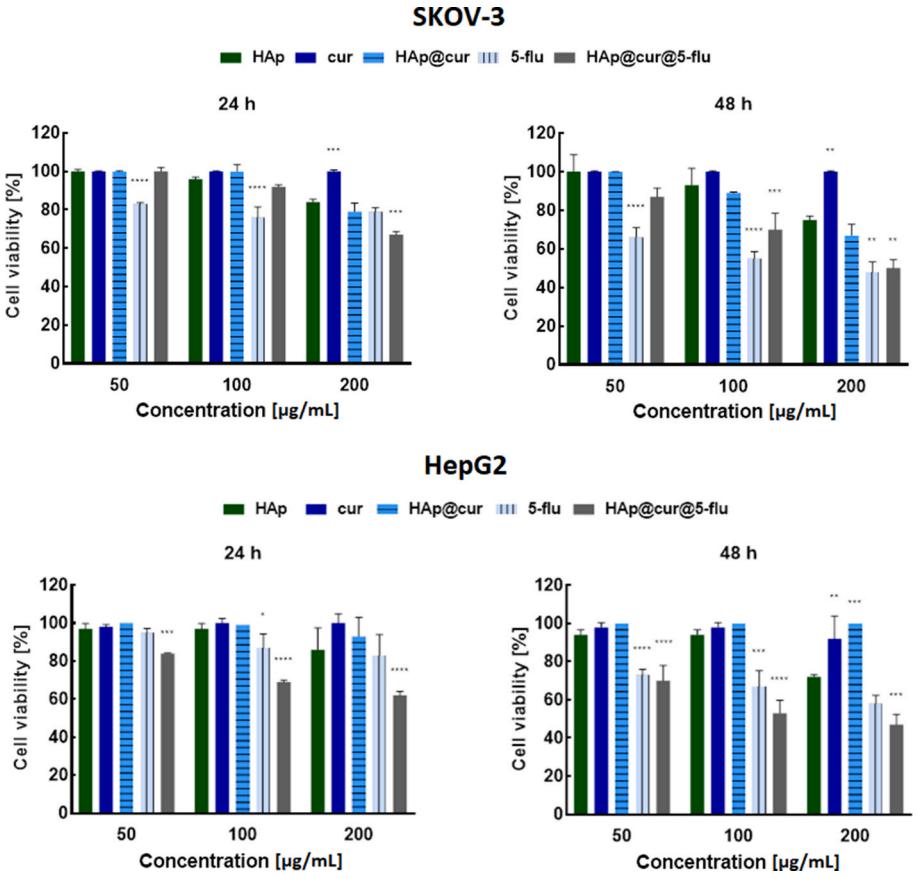

Fig. 9. Cytotoxicity studies performed on SKOV-3 and HepG2 cells treated with various concentrations (50, 100, 200 μM) of HAp, cur, HAp@cur, 5-flu, HAp@cur@5-flu after 24 h and 48 h of incubation. Data points and SD are from at least three measurements. Statistical significance was considered if $p \leq 0.05$ (*), $p \leq 0.01$ (**), $p \leq 0.001$ (***), $p \leq 0.0001$ (****).

Table 2
IC50 values for HAp@cur@5-flu and 5-flu on both cell lines.

	24 h		48 h	
	HepG2	SKOV-3	HepG2	SKOV-3
HAp@cur@5-flu	42.56 μg mL^{-1}	89.44 μg mL^{-1}	20.67 μg mL^{-1}	30.33 μg mL^{-1}
5-flu	135.0 μg mL^{-1}	75.35 μg mL^{-1}	33.14 μg mL^{-1}	25.56 μg mL^{-1}

through the desorption of the adsorbed drug from the curcuminoids-stabilized-hydroxyapatite. The process can undergo via diffusion of a 5-fluorouracil from the matrix of the drug carrier to the cancer cells or osmotic pumping [26,116]. It has been documented that factors such as pH, drug solubility, and temperature among other factors, influence the release of drugs [117].

4. Conclusions

In this work, we demonstrated the colloidal suspension based on the nanostructural hydroxyapatite loaded with natural plant extract and the anticancer drug for the cancer cells treatment. The hydroxyapatite nanocarrier was synthesized with co-precipitating method as a porous platform facile to be loaded with thearapeutic agents. HAp was obtained in rod-like shape and nanometric size offering large surface-to-volume ratio and stabilized with curcuminoids extracted from *Curcuma longa* L. rhizome. The extract was used for its enriched composition in contrast to the commercially available curcumin, containing even nine biologically active compounds. The chemical composition of the extract was studied with HPLC and GC confirming the revealing presence of even nine biologically active compounds. The extract was proposed to improve the anticancer effect of the composite, while it also worked well as a stabilizing agent of nanocomposite. Proposed nanocomposite was also loaded with 5-fluorouracil anticancer drug and the nanocomposite was tested within the Langmuir trough to determine the interaction of the nanocomposite with biomimetic membranes. The relatively specific surface of HAp is also contributed to its better loading of the drug, while the effect differs depending on the type of carrier modification. The presence of curcuminoids in the hydroxyapatite changes the surface properties of the conjugate, which contributes to the low affinity of the nanocarrier to most of the tested membranes. The 5-fluorouracil shows an accumulation in the structure of the lipids tested, but the use of hydroxyapatite as a carrier significantly reduces this type of interaction, while still, the nanocomposite interacts with biomimetic membranes.

Then, the nanocomposite loaded with a drug was tested *in vitro* on SKOV-3 and HepG2 cancer cells to check its cytotoxicity. It can be seen that the nanocomposite reveals the therapeutic effect towards both cancer cells confirming its potential to be applied in anticancer therapy. Depending on the cell type the nanocomposite uptake differs what shows the potential for the particular cancer types treatment.

Funding sources

This work was supported by the Vietnam Academy of Science and Technology under grant No. CT0000.09/21-23.

Declaration of competing interest

The authors declare that they have no known competing financial interests or personal relationships that could have appeared to influence the work reported in this paper.

Acknowledgements

Sunday J. Olusegun with No PPN/ULM/2020/1/00051/DEC/01, would like to thank the NAWA - Narodowa Agencja Wymiany Akademickiej (Polish National Agency for Academic Exchange) for their support.

References

[1] S. Naahidi, M. Jafari, F. Edalat, K. Raymond, A. Khademhosseini, P. Chen, Biocompatibility of engineered nanoparticles for drug delivery, J. Contr. Release 166 (2013) 182–194, https://doi.org/10.1016/j.jconrel.2012.12.013.
[2] M.M.A.N. Ranjha, B. Shafique, A. Rehman, A. Mehmood, A. Ali, S.M. Zahra, U. Roobab, A. Singh, S.A. Ibrahim, S.A. Siddiqui, Biocompatible nanomaterials in food science, technology, and nutrient drug delivery: recent developments and applications, Front. Nutr. 8 (2022) 1–15, https://doi.org/10.3389/fnut.2021.778155.
[3] H. Zhou, J. Lee, Nanoscale hydroxyapatite particles for bone tissue engineering, Acta Biomater. 7 (2011) 2769–2781, https://doi.org/10.1016/j.actbio.2011.03.019.
[4] S. Ram Prasad, A. Jayakrishnan, T.S. Sampath Kumar, Hydroxyapatite-Poly(Vinyl alcohol) core-shell nanoparticles for dual delivery of methotrexate and gemcitabine for bone cancer treatment, J. Drug Deliv. Sci. Technol. 51 (2019) 629–638, https://doi.org/10.1016/j.jddst.2019.03.041.
[5] J. Song, N. Cui, X. Mao, Q. Huang, E.S. Lee, H. Jiang, Sorption studies of tetracycline antibiotics on hydroxyapatite (001) surface—a first-principles insight, Materials 15 (2022), https://doi.org/10.3390/ma15030797.
[6] S. Mondal, S.V. Dorozhkin, U. Pal, Recent progress on fabrication and drug delivery applications of nanostructured hydroxyapatite, Wiley Interdiscip. Rev. Nanomedicine Nanobiotechnology 10 (2018) 1–32, https://doi.org/10.1002/wnan.1504.
[7] A. Szcześ, L. Hołysz, E. Chibowski, Synthesis of hydroxyapatite for biomedical applications, Adv. Colloid Interface Sci. 249 (2017) 321–330, https://doi.org/10.1016/j.cis.2017.04.007.
[8] P. Sobierajska, A. Dorotkiewicz-Jach, K. Zawisza, J. Okal, T. Olszak, Z. Drulis-Kawa, R.J. Wiglusz, Preparation and antimicrobial activity of the porous hydroxyapatite nanoceramics, J.Alloys Compound 748 (2018) 179–187, https://doi.org/10.1016/j.jallcom.2018.03.162.
[9] K. Zawisza, P. Sobierajska, N. Nowak, A. Kedziora, K. Korzekwa, B. Pozniak, M. Tikhomirov, J. Miller, L. Mrowczynska, R.J. Wiglusz, Preparation and preliminary evaluation of bio-nanocomposites based on hydroxyapatites with antibacterial properties against anaerobic bacteria, Mater. Sci. Eng. C 106 (2020), 110295, https://doi.org/10.1016/j.msec.2019.110295.
[10] D.A.C. Ferreira-Ermita, F.L. Valente, E.C. Carlo-Reis, F.R. Araújo, I.M. Ribeiro, C. C.V. Cintra, A.P.B. Borges, Characterization and in vivo biocompatibility analysis of synthetic hydroxyapatite compounds associated with magnetite nanoparticles for a drug delivery system in osteomyelitis treatment, Results Mater 5 (2020), https://doi.org/10.1016/j.rinma.2020.100063.
[11] D. Lee, M. Wufuer, I. Kim, T.H. Choi, B.J. Kim, H.G. Jung, B. Jeon, G. Lee, O. H. Jeon, H. Chang, D.S. Yoon, Sequential dual-drug delivery of BMP-2 and alendronate from hydroxyapatite-collagen scaffolds for enhanced bone regeneration, Sci. Rep. 11 (2021) 1–10, https://doi.org/10.1038/s41598-020-80608-3.
[12] C. Vásquez-López, M.M. Castillo-Ortega, L.H. Chan-Chan, I. Lagarda-Díaz, A. L. Giraldo-Betancur, D.E. Rodríguez-Félix, J.C. Encinas-Encinas, M.E. Martínez-Barbosa, G. Cadenas-Pliego, J.V. Cauich-Rodríguez, P.J. Herrera-Franco, Polyurethane electrospun membranes with hydroxyapatite-vancomycin for potential application in bone tissue engineering and drug delivery, J. Appl. Polym. Sci. 139 (2022), https://doi.org/10.1002/app.51893.
[13] W. Sun, J. Fan, S. Wang, Y. Kang, J. Du, X. Peng, Biodegradable drug-loaded hydroxyapatite nanotherapeutic agent for targeted drug release in tumors, ACS Appl. Mater. Interfaces 10 (2018) 7832–7840, https://doi.org/10.1021/acsami.7b19281.
[14] R.C.R. Apostolos, M.C. De Miranda, W.M. Silva, D. de A. Gomes, M.C. de Miranda, E.M.B. de Sousa, Hybrid polymeric systems of mesoporous silica/hydroxyapatite nanoparticles applied as antitumor drug delivery platform, Int. J. Appl. Ceram. Technol. 16 (2018) 1836–1849, https://doi.org/10.1111/ijac.13231.
[15] Q. Zhao, D. Zhang, R. Sun, S. Shang, H. Wang, Y. Yang, L. Wang, X. Liu, T. Sun, K. Chen, Adsorption beahavior of drug on hydroxyapatite with different morphologies: a combined experimental and molecular dynamics simulation study, Ceram. Int. 45 (2019) 19522–19527, https://doi.org/10.1016/j.ceramint.2019.06.068.
[16] X. Jiang, Y. Zhao, C. Wang, R. Sun, Y. Tang, Effects of physico-chemical properties of ions-doped hydroxyapatite on adsorption and release performance of doxorubicin as a model anticancer drug, Mater. Chem. Phys. 276 (2022), 125440, https://doi.org/10.1016/j.matchemphys.2021.125440.
[17] K. Watanabe, Y. Nishio, R. Makiura, A. Nakashira, C. Kojima, Paclitaxel-loaded hydroxyapatite/collagen hybrid gels as drug delivery systems for metastatic cancer cells, Int. J. Pharm. 446 (2013) 81–86, https://doi.org/10.1016/j.ijpharm.2013.02.002.
[18] J. Vechasilp, B. Tangtrakulwanich, K. Oungbho, S. Yuenyongsawad, The efficacy of methotrexate-impregnated hydroxyapatite composites on human mammary carcinoma cells, J. Orthop. Surg. 15 (2007) 56–61, https://doi.org/10.1177/230949900701500113.
[19] P. Sobierajska, A. Serwotka-Suszczak, S. Targonska, D. Szymanski, K. Marycz, R. J. Wiglusz, Synergistic effect of toceranib and nanohydroxyapatite as a drug delivery platform—physicochemical properties and in vitro studies on mastocytoma cells, Int. J. Mol. Sci. 23 (2022) 1944, https://doi.org/10.3390/ijms23041944.

[20] H. Luo, D. Ji, C. Li, Y. Zhu, G. Xiong, Y. Wan, Layered nanohydroxyapatite as a novel nanocarrier for controlled delivery of 5-fluorouracil, Int. J. Pharm. 513 (2016) 17–25, https://doi.org/10.1016/j.ijpharm.2016.09.004.
[21] K. Grocholewicz, G. Matkowska-Cichocka, P. Makowiecki, A. Droździk, H. Ey-Chmielewska, A. Dziewulska, M. Tomasik, G. Trybek, J. Janiszewska-Olszowska, Effect of nano-hydroxyapatite and ozone on approximal initial caries: a randomized clinical trial, Sci. Rep. 10 (2020) 1–8, https://doi.org/10.1038/s41598-020-67885-8.
[22] J. Xu, M. Liao, Y. Chen, L. Chen, Novel fabrication of marizomib-loaded chitosan-coated hydroxyapatite nanocarriers as a promising system for effective treatment of ovarian cancer mater, Res. Express. 9 (2022) 1–12, https://doi.org/10.1088/2053-1591/ac5077.
[23] M. del Carmen De Lama-Odría, L.J. del Valle, J. Puiggalí, Hydroxyapatite biobased materials for treatment and diagnosis of cancer, Int. J. Mol. Sci. 23 (2022) 1–35, 10.339/ijms231922352.
[24] C. Santos, C.F. Rovath, R.-P. Franke, M.M. Almeida, M.E.V. Costa, Spray-dried hydroxyapatite-5-Fluorouracil granules as a chemotherapeutic delivery system, Ceram. Int. 35 (2009) 509–513, https://doi.org/10.1016/j.ceramint.2008.01.012.
[25] Y. Ji, A. Wang, G. Wu, H. Yin, S. Liu, B. Chen, F. Liu, X. Li, Synthesis of different sized and porous hydroxyapatite nanorods without organic modifiers and their 5-fluorouracil release performance, Mater. Sci. Eng. C 57 (2015) 14–25, https://doi.org/10.1016/j.msec.2015.07.008.
[26] Ch-L. Tseng, J.-Ch Chen, Y.-Ch Wu, H.-W. Fang, F.-H. Lin, T.-P. Tang, Development of lattice-inserted 5-fluorouracil-hydroxyapatite nanoparticles as a chemotherapeutic delivery system, 30, https://doi.org/10.1177/088532821558, 2015.
[27] B. Kundu, D. Ghosh, M.K. Sinha, P.S. Sen, V.K. Balla, N. Das, D. Basu, Doxorubicin-intercalated nano-hydroxyapatite drug-delivery system for liver cancer: an animal model, Ceram. Int. 39 (2013) 9557–9566, https://doi.org/10.1016/j.ceramint.2013.05.074.
[28] Ch-T. Yang, K.-Y. Li, F.-Q. Meng, J.-F. Lin, I.-Ch Young, R. Ivkov, F.-H. Lin, ROS-induced HepG2 cell death from hyperthermia using magnetic hydroxyapatite nanoparticles, Nanotechnology 37 (2018), https://doi.org/10.1088/1361-6528/aacda1.
[29] N.S. Awwad, A.M. Alshahrani, K.A. Saleh, M.S. Hamdy, Novel method to improve the anticancer activity of natural-based hydroxyapatite against the liver cancer cell line HepG2 using mesoporous magnesia as a micro-carrier, Molecules 22 (2017) 1–11, https://doi.org/10.3390/molecules22121947.
[30] S. Gao, Y. Lin, M. Zheng, Y. Lin, K. Lin, S. Xie, Y. Yu, J. Lin, Label-free determination of liver cancer stages using surface-enhanced Raman scattering coupled with preferential adsorption of hydroxyapatite microspheres, Anal. Methods 13 (2021) 3885–3893, https://doi.org/10.1039/D1AY00946J.
[31] M. Tantawy, A. Wilson, A. Beeghly-Fadiel, F. Yull, J. Gore, R. Alvarez, M. Crispens, J. O. McIntyre, Tumor Extracellular Hydroxyapatite: a Potential Biomarker for Imaging Ovarian Cancer, Gynecol. Oncol., 162(202), 318-332 https://doi.org/10.1016/S0090-8258(21)01255-5.
[32] R. Chyzhma, A. Piddubnyi, S. Danilchenko, O. Kravtsova, R. Moskalenko, Potential role of hydroxyapatite nanocrystalline for early diagnostics of ovarian cancer, Diagnostics 11 (2021) 1–12, https://doi.org/10.3390/diagnostics11101741.
[33] E.W. Elsayed, A.A. El-Ashmawy, G.T. El-Bassyouni, S.M. Mousa, M. El-Manawaty, L.H. Emara, Formulation and evaluation ofAalginate-gelatin hydrogel scaffolds loaded with zinc-doped hydroxyapatite and 5-fluorouracil, Int. J. Biol. Macromol. 15 (2023), https://doi.org/10.1016/j.ijbiomac.2023.124147.
[34] D. Weerasuriya, W. Wijesinghe, R. Rajapakse, Encapsulation of anticancer drug copper bis(8-hydroxyquinoline) in hydroxyapatite for pH-sensitive targeted delivery and slow release, Mater. Sci. Eng. C 71 (2017) 206–213, https://doi.org/10.1016/j.msec.2016.10.010.
[35] W. Sun, J. Fan, S. Wang, Y. Kang, J. Du, X. Peng, Biodegradable drug-loaded hydroxyapatite nanotherapeutic agent for targeted drug release in tumors, Appl. Mater. Interfaces 10 (2018) 7832–7840, https://doi.org/10.1021/acsami.7b19281.
[36] M. Préfontaine, J.T. Donovan, J.L. Powell, L. Buley, Treatment of refractory ovarian cancer with 5-fluorouracil and leucovorin, Gynecol. Oncol. 61 (1996) 249–252, https://doi.org/10.1006/gyno.1996.0134.
[37] S. Sato, H. Itamochi, J. Kigawa, T. Oishi, M. Shimada, S. Sato, J. Naniwa, K. Uegaki, M. Nonaka, N. Terakawa, Combination chemotherapy of oxaliplatin and 5-fluorouracil may be an effective regimen for mucinous adenocarcinoma of the ovary: a potential treatment strategy, Cancer Sci. 100 (2009) 546–551, https://doi.org/10.1111/j.1349-7006.2008.01065.
[38] S. Salerno, A. Ståhlberg, A. Holdfeldt, E.B. Lindskog, G. Landberg, 5-Fluorouracil treatment of patient-derived scaffolds from colorectal cancer reveal clinically critical information, J. Transl. Med. 20 (2022) 1–13, https://doi.org/10.1186/s12967-022-03423-6.
[39] Y. Gao, X. Xiao, C. Zhang, W. Yu, W. Guo, Z. Zhang, Z. Li, X. Feng, J. Hao, K. Zhang, B. Xiao, M. Chen, W. Huang, S. Xiong, X. Wu, W. Deng, Melatonin synergizes the chemotherapeutic effect of 5-fluorouracil in colon cancer by suppressing PI3K/AKT and NF-κB/iNOS signaling pathways, J. Pineal Res. 2 (2017), https://doi.org/10.1111/jpi.12380.
[40] W. Wang, Y. Yang, Y.-P. Zhao, T.-P. Zhang, Q. Liao, H. Shu, Recent studies of 5-fluorouracil resistance in pancreatic cancer, World J. Gastroenterol. 20 (2014) 15682–15690, https://doi.org/10.3748/wjg.v20.i42.15682.
[41] H. Burris, A.M. Storniolo, Assessing clinical benefit in the treatment of pancreas cancer: gemcitabine compared to 5-fluorouracil, Eur. J. Cancer 33 (1997) S18–S22, https://doi.org/10.1016/S0959-8049(96)00324-.
[42] M. Nasr, M.K. Ghora, A. Abdelazem, In vitro and in vivo evaluation of cubosomes containing 5-fluorouracil for liver targeting, Acta Pharm. Sin. B 5 (2015) 79–88, https://doi.org/10.1016/j.apsb.2014.12.001.
[43] L.F. Lai, H.X. Guo, Preparation of new 5-fluorouracil-loaded zein nanoparticles for liver targeting, Int. J. Pharm. 404 (2011) 317–323, https://doi.org/10.1016/j.ijpharm.2010.11.025.
[44] K. Tecza, J. Pamula-Pilat, J. Lanuszewska, D. Butkiewicz, E. Grzybowska, Pharmacogenetics of toxicity of 5-fluorouracil, doxorubicin and cyclophosphamide chemotherapy in breast cancer patients, Oncotarget 10 (2018) 9114–9136, https://doi.org/10.18632/oncotarget.24148.
[45] J. Tian, D. Zhang, V. Kurbatov, Q. Wang, D. Fang, L. Wu, M. Bosenberg, M. D. Muzumdar, S. Khan, Q. Lu, Q. Yan, J. Lu, 5-fluorouracil efficacy requires anti-tumor immunity triggered by cancer-cell-intrinsic STING, EMBO J. 40 (2021), e106065, https://doi.org/10.15252/embj.2020106065.
[46] E. Chu, G.M. Lai, S. Zinn, C.J. Allegra, Resistance of a human ovarian cancer line to 5-fluorouracil associated with decreased levels of 5-fluorouracil in DNA, Mol. Pharmacol. 3 (1990) 410–417.
[47] G. Bocci, C. Barbara, F. Vannozzi, A. Di Paolo, A. Melosi, G. Barsanti, G. Allegrini, A. Falcone, M. Del Tacca, R. Danesi, A pharmacokinetic-based test to prevent severe 5-fluorouracil toxicity, Clin. Pharmacol. Ther. 80 (2006) 384–395, https://doi.org/10.1016/j.clpt.2006.06.007.
[48] J.J. Lee, J.H. Beumer, E. Chu, Therapeutic drug monitoring of 5-fluorouracil, Cancer Chemother. Pharmacol. 78 (2016) 447–464, https://doi.org/10.1007/s00280-016-3054-2.
[49] Y. Wei, P. Yang, S. Cao, L. Zhao, The combination of curcumin and 5-fluorouracil in cancer therapy, Arch Pharm. Res. (Seoul) 41 (2018) 1–13, https://doi.org/10.1007/s12272-017-0979-x.
[50] Y. Pan, R. Ju, X. Cao, H. Pei, T. Zheng, W. Wang, Optimization extraction and purification of biological activity curcumin from Curcuma longa L by high-performance counter-current chromatography, J. Separ. Sci. 43 (2020) 1586–1592, https://doi.org/10.1002/jssc.201901174.
[51] P. Degot, V. Huber, E. Hofmann, M. Hahn, D. Touraud, W. Kunz, Solubilization and extraction of curcumin from Curcuma longa using green, sustainable, and food-approved surfactant-free microemulsions, Food Chem. 336 (2021), 127660, https://doi.org/10.1016/j.foodchem.2020.127660.
[52] S. Hadi, A.N. Artanti, Y. Rinanto, D.S.C. Wahyuni, Curcuminoid content of Curcuma longa L. And Curcuma xanthorrhiza rhizome based on drying method with NMR and HPLC-UVD, Mater. Sci. Eng. 567 (2018) 7–12, https://doi.org/10.1088/1757-899X/349/1/012058.
[53] N. Nurjanah, E. Saepudina, Curcumin isolation, synthesis and characterization of curcumin isoxazole derivative compound, AIP Conf. Proc. 2168 (2020), 020065.
[54] J. Akter, A. Hossain, K. Takara, Z. Islam, Comparative biochemistry and physiology, Part C antioxidant activity of di ff erent species and varieties of turmeric (Curcuma spp): isolation of active compounds, Comp. Biochem. Physiol., C 215 (2019) 9–17, https://doi.org/10.1016/j.cbpc.2018.09.002.
[55] S. Khan, M. Imran, T. Tahir, S. Wadood, A. Shah, M. Sohail, A. Malik, S. Das, H. Ei, A. Adam, Z. Hussain, Curcumin Based Nanomedicines as e Ffi Cient Nanoplatform for Treatment of Cancer : new Developments in Reversing Cancer Drug Resistance, Rapid Internalization, and Improved Anticancer Efficacy, Trends Food Sci. Technol. 80 (2018) 8–22, https://doi.org/10.1016/j.tifs.2018.07.026.
[56] A. Mukerjee, J.K. Vishwanatha, Formulation, characterization and evaluation of curcumin-loaded PLGA nanospheres for cancer therapy, Anticancer Res. 3876 (2009) 3867–3875.
[57] H.H.M. San, K.P. Alcantara, B.P.I. Bulatao, W. Chaichompoo, N. Nalinratana, A. Suksamrarn, O. Vajragupta, P. Rojsitthisak, P. Rojsitthisak, Development of turmeric oil—loaded chitosan/alginate nanocapsules for cytotoxicity enhancement against breast cancer, Polymers 14 (2022), https://doi.org/10.3390/polym14091835.
[58] I.-C. Chao, C.-M. Wang, S.-P. Li, L.-G. Lin, W.-C. Ye, Q.-W. Zhang, Simultaneous quantification of three curcuminoids and three volatile components of Curcuma longa using pressurized liquid extraction and high-performance liquid chromatography, Molecules 23 (2018) 1568, https://doi.org/10.3390/molecules23071568.
[59] S. Wilczewski, K. Skórczewska, J. Tomaszewska, K. Lewandowski, W. Studziński, M. Osial, P. Jenczyk, H. Grzywacz, A. Domańska, Curcuma longa L. Rhizome extract as a poly(vinyl chloride)/graphene nanocomposite green modifier, Molecules 27 (2022) 8081, https://doi.org/10.3390/molecules27228081.
[60] S. Fuloria, J. Mehta, A. Chandel, M. Sekar, N.N.I.M. Rani, M.Y. Begum, V. Subramaniyan, K. Chidambaram, L. Thangavelu, R. Nordin, Y.S. Wu, K. V. Sathasivam, P.T. Lum, D.U. Meenakshi, V. Kumarasamy, A.K. Azad, N.K. A. Fuloria, Comprehensive review on the therapeutic potential of Curcuma longa linn. In relation to its major active constituent curcumin, Front. Pharmacol. 13 (2022) 1–27, https://doi.org/10.3389/fphar.2022.820806.
[61] D.K. Poudel, P.K. Ojha, A. Rokaya, R. Satyal, P. Satyal, W.N. Setzer, Analysis of volatile constituents in Curcuma species, viz. C. Aeruginosa, C. Zedoaria, and C. Longa, from Nepal, Plants 11 (2022) 1–12, https://doi.org/10.3390/plants11151932.
[62] M. Radice, N.R. Maddela, L. Scalvenzi, Biological activities of zingiber officinale roscoe essential oil against Fusarium spp.: a minireview of a promising tool for biocontrol, Agronomy 12 (2022), https://doi.org/10.3390/agronomy12051168.
[63] S. Kothapally, S. Alukapally, N. Nagula, R. Maddela, Superior bioavailability of a novel curcumin formulation in healthy humans under fasting conditions, Adv. Ther. 39 (2022) 2128–2138, https://doi.org/10.1007/s12325-022-02081-w.
[64] H. Xiang, L. Zhang, Z. Yang, F. Chen, X. Zheng, X. Liu, Chemical compositions, antioxidative, antimicrobial, anti-inflammatory and antitumor activities of

Curcuma aromatica Salisb. essential oils, Ind. Crop. Prod. 108 (2017) 6–16, https://doi.org/10.1016/j.indcrop.2017.05.058.
[65] K.M. Nelson, J.L. Dahlin, J. Bisson, J. Graham, G.F. Pauli, M.A. Walters, The essential medicinal chemistry of curcumin, J. Med. Chem. 60 (2017) 1620–1637, https://doi.org/10.1021/acs.jmedchem.6b00975.
[66] H. Hatcher, R. Planalp, J. Cho, F.M. Torti, S.V. Torti, Curcumin: from ancient medicine to current clinical trials, Cell. Mol. Life Sci. 65 (2008) 1631–1652, https://doi.org/10.1007/s00018-008-7452-4.
[67] B. Salehi, Z. Stojanović-Radić, J. Matejić, M. Sharifi-Rad, N.V. Anil Kumar, N. Martins, J. Sharifi-Rad, The therapeutic potential of curcumin: a review of clinical trials, Eur. J. Med. Chem. 163 (2019) 527–545, https://doi.org/10.1016/j.ejmech.2018.12.016.
[68] R. Li, C. Xiang, X. Zhang, D. An Guo, M. Ye, Chemical analysis of the Chinese herbal medicine turmeric (Curcuma longa L.), Curr. Pharmaceut. Anal. 6 (4) (2010) 256–268, https://doi.org/10.2174/157341210793292356.
[69] L. lu Xu, Z. peng Shang, Y. ying Lu, P. Li, L. Sun, Q. lei Guo, T. Bo, Z. yong Le, Z. li Bai, X. li Zhang, X. Qiao, M. Ye, Analysis of curcuminoids and volatile components in 160 batches of turmeric samples in China by high-performance liquid chromatography and gas chromatography mass spectrometry, J. Pharm. Biomed. Anal. 188 (2020) 1–7, https://doi.org/10.1016/j.jpba.2020.113465.
[70] D. Núñez, J.A. Serrano, A. Mancisidor, E. Elgueta, K. Varaprasad, P. Oyarzún, R. Cáceres, W. Ide, B.L. Rivas, Heavy metal removal from aqueous systems using hydroxyapatite nanocrystals derived from clam shells, RSC Adv. 9 (2019) 22883–22890, https://doi.org/10.1039/c9ra04198b.
[71] M. Mujahid, S. Sarfraz, S. Amin, On the formation of hydroxyapatite nano crystals prepared using cationic surfactant, Mater. Res. 18 (2015) 468–472, https://doi.org/10.1590/1516-1439.298014.
[72] S. Sebastiammal, A.S.L. Fathima, S. Devanesan, M.S. AlSalhi, J. Henry, M. Govindarajan, B. Vaseeharan, Curcumin-encased hydroxyapatite nanoparticles as novel biomaterials for antimicrobial, antioxidant and anticancer applications: a perspective of nano-based drug delivery, J. Drug Deliv. Sci. Technol. 57 (2020), 101752, https://doi.org/10.1016/j.jddst.2020.101752.
[73] M.B. Febrian, I. Mahendra, A. Kurniawan, Y. Setiadi, T.H.A. Wibawa, R. Lesmana, D.G. Syarif, Zirconium doped hydroxyapatite as a potential design for lung therapy, Ceram. Int. 47 (2021) 27890–27897, https://doi.org/10.1016/j.ceramint.2021.06.219.
[74] X.Y. Zhao, I.J. Zhu, C. Qi, F. Chen, B.Q. Lu, J. Zhao, J. Wu, Hierarchical hollow hydroxyapatite microspheres: microwave-assisted rapid synthesis by using pyridoxal-5′-phosphate as a phosphorus source and application in drug delivery, Chem. Asian J. 8 (2013) 1313–1320, https://doi.org/10.1002/asia.201300142.
[75] A. Serhiienko, T. Dontsova, O. Yanushevska, A. Lapinskyi, G. Krymets, Synthesis and characterization of hydroxyapatite and composite based on it with collagen/alginate, Chem. Pap. 76 (2022) 385–392, https://doi.org/10.1007/s11696-021-01841-2.
[76] A. Rout, S. Agrawal, Structural, morphological and electrical properties of new type Dy doped $Ca_{6-x}Na_2Y_2(SiO_4)_6(OH)_2$ hydroxyapatite compound synthesized by Co – precipitation method, J. Electroceram. 48 (2022) 74–94, https://doi.org/10.1007/s10832-021-00274-3.
[77] C. Ragunath, L. Kousalya, R. Venkatachalam, S. Anitha, Green synthesis of hydroxyapatite nanoparticles from wrightia tinctoria and its antibacterial activity, Bionanoscience 12 (2022) 723–730, https://doi.org/10.1007/s12668-022-01012-x.
[78] T. Scharnweber, C. Santos, R.-P. Franke, M.M. Almeida, E.M. Costa, Influence of spray-dried hydroxyapatite-5-fluorouracil granules on cell lines derived from tissues of mesenchymal origin, Molecules 13 (2008) 2729–2739, https://doi.org/10.3390/molecules13112729.
[79] M. Shaban, M.R. Abukhadra, A.S. Mohamed, M.G. Shahien, S.S. Ibrahim, Synthesis of mesoporous graphite functionalized by nitrogen for efficient removal of safranin dye utilizing rice husk ash; equilibrium studies and response surface optimization, J. Inorg. Organomet. Polym. Mater. 28 (2018) 279–294, https://doi.org/10.1007/s10904-017-0726-2.
[80] P.T. Nguyen, X.T. Nguyen, T.V. Nguyen, T.T. Nguyen, T.Q. Vu, H.T. Nguyen, N. T. Pham, T.M. Thi Dinh, Treatment of Cd2+ and Cu2+ ions using modified apatite ore, J. Chem. (2020), https://doi.org/10.1155/2020/6527197, 2020.
[81] O. Ayodele, S.J. Olusegun, O.O. Oluwasina, E.A. Okoronkwo, L. Beatriz, E. O. Olanipekun, N.D.S. Mohallem, W.G. Guimar, F.D.M. Gomes, G.D.O. Souza, A. Duarte, Experimental and theoretical studies of the adsorption of Cu and Ni ions from wastewater by hydroxyapatite derived from eggshells, Environ. Nanotechnol. Monit. Manag. 15 (2021), https://doi.org/10.1016/j.enmm.2021.100439.
[82] P. Sobierajska, R.J. Wiglusz, Influence of Li+ ions on the physicochemical properties of nanocrystalline calcium–strontium hydroxyapatite doped with Eu3 + ions, New J. Chem. 43 (2019) 14908–14916, https://doi.org/10.1039/C9NJ03003D.
[83] A. Slosarczyka, Z. Paszkiewicza, C. Paluszkiewicz, FTIR and XRD evaluation of carbonated hydroxyapatite powders synthesized by wet methods, J. Mol. Struct. 747 (2005) 657–661, https://doi.org/10.1016/j.molstruc.2004.11.078, 744–747.
[84] H. Gheisari, E. Karamian, M. Abdellahi, A novel hydroxyapatite-hardystonite nanocomposite ceramic, Ceram. Int. 41 (2015) 5967–5975, https://doi.org/10.1016/j.ceramint.2015.01.033.
[85] P.N. Nam, N.T. Thom, N.T. Phuong, N.T. Xuyen, N.S. Hai, N.T. Anh, P.T. Dung, D. T.M. Thanh, Synthesis, Characterization and Antimicrobial Activity of Copper Doped Hydroxyapatite, vol. 56, 2018, pp. 672–678, https://doi.org/10.1002/vjch.201800068.
[86] N.T. Thom, P.T. Nam, N.T. Phuong, C.T. Hong, N.V. Trang, N.T. Xuyen, D.T. M. Thanh, Electrodeposition of hydroxyapatite/functionalized carbon nanotubes (HAp/fCNTs) coatings on the surface of 316L stainless steel, Vietnam J. Sci. Technol. 55 (2017) 706–715, https://doi.org/10.15625/2525-2518/55/6/9153.
[87] G. Zuo, Y. Wan, X. Meng, Q. Zhao, K. Ren, S. Jia, J. Wang, Synthesis and characterization of a lamellar hydroxyapatite/DNA nanohybrid, Mater. Chem. Phys. 126 (2011) 470–475, https://doi.org/10.1016/j.matchemphys.2010.12.060.
[88] X. Chen, L.Q. Zou, J. Niu, W. Liu, S.F. Peng, C.M. Liu, The stability, sustained release and cellular antioxidant activity of curcumin nanoliposomes, Molecules 20 (2015) 14293–14311, https://doi.org/10.3390/molecules200814293.
[89] E.H. Ismail, D.Y. Sabry, H. Mahdy, M.M.H. Khalil, Synthesis and characterization of some ternary metal complexes of curcumin with 1,10-phenanthroline and their anticancer applications, J. Sci. Res. 6 (2014) 509–519, https://doi.org/10.3329/jsr.v6i3.18750.
[90] K.K. Gupta, N. Pal, P.K. Mishra, P. Srivastava, S. Mohanty, P. Maiti, 5-Florouracil-Loaded poly(lactic acid)-poly(caprolactone) hybrid scaffold: potential chemotherapeutic implant, J. Biomed. Mater. Res., Part A 102 (2014) 2600–2612, https://doi.org/10.1002/jbm.a.34932.
[91] L. Jin, Q. Liu, Z. Sun, X. Ni, M. Wei, Preparation of 5-Fluorouracil/β-Cyclodextrin complex intercalated in layered double hydroxide and the controlled drug release properties, Ind. Eng. Chem. Res. 49 (2010) 11176–11181, https://doi.org/10.1021/ie100990z.
[92] J. Jin, G. Zuo, G. Xiong, H. Luo, Q. Li, C. Ma, D. Li, F. Gu, Y. Ma, Y. Wan, The inhibition of lamellar hydroxyapatite and lamellar magnetic hydroxyapatite on the migration and adhesion of breast cancer cells, J. Mater. Sci. Mater. Med. 25 (2014) 1025–1031, https://doi.org/10.1007/s10856-013-5126-8.
[93] H.D. Rajapakse, S.U. Adikary, Synthesis and Characterization of Chitosan/hydroxyapatite Nanocomposite for Bone Tissue Engineering Applications, IEEE, 2021, 9781665437530.45.
[94] A. Slavov, I. Panchev, D. Kovacheva, I. Vasileva, Physico-chemical characterization of water-soluble pectic extracts from Rosa damascena, Calendula officinalis and Matricaria chamomilla wastes, Food Hydrocolloids 61 (2016) 469–476, https://doi.org/10.1016/j.foodhyd.2016.06.006.46.
[95] A. Gupta, G. Tiwari, R. Tiwari, R. Srivastava, Factorial designed 5-fluorouracil-loaded microsponges and calcium pectinate beads plugged in hydroxypropyl methylcellulose capsules for colorectal cancer, Int. J. Pharm. Investig. 5 (2015) 234, https://doi.org/10.4103/2230-973x.167688.
[96] J. Dai, G. Wang, L. Ma, C. Wu, Study on the surface energies and dispersibility of graphene oxide and its derivatives, J. Mater. Sci. 50 (2015) 3895–3907, https://doi.org/10.1007/s10853-015-8934-z.
[97] Z. Zhong, K. Woo, I. Kim, H. Hwang, S. Kwon, Y.M. Choi, Y. Lee, T.M. Lee, K. Kim, J. Moon, Roll-to-Roll-Compatible, flexible, transparent electrodes based on self-nanoembedded Cu nanowires using intense pulsed light irradiation, Nanoscale 8 (2016) 8995–9003, https://doi.org/10.1039/c6nr00444j.
[98] Z. Lili, Z. Hongfei, S. Shoukat, Z. Xiaochen, Z. Bolin, Screening lactic acid bacteria strains with ability to bind di-n-butyl phthalate via turbiscan technique. Antonie van Leeuwenhoek, Int. J. Gen. Mol. Microbiol. 110 (2017) 759–769, https://doi.org/10.1007/s10482-017-0846-2.
[99] J.W. Lee, S.W. Kim, Y.L. Cho, H.Y. Jeong, Y. Il Song, S.J. Suh, Dispersion stabilities of multi-layer graphene-coated copper prepared by electrical wire-explosion method, J. Nanosci. Nanotechnol. 16 (2016) 11286–11291, https://doi.org/10.1166/jnn.2016.13495.
[100] X. Qi, Y. Dong, H. Wang, C. Wang, F. Li, Application of turbiscan in the homoaggregation and heteroaggregation of copper nanoparticles, Colloids Surfaces A Physicochem. Eng. Asp. 535 (2017) 96–104, https://doi.org/10.1016/j.colsurfa.2017.09.015.
[101] M. Elderdfi, A.F. Sikorski, Langmuir-monolayer methodologies for characterizing protein-lipid interactions, Chem. Phys. Lipids 212 (2018) 61–72, https://doi.org/10.1016/j.chemphyslip.2018.01.008.
[102] C. Peetla, S. Jin, J. Weimer, A. Elegbede, V. Labhasetwar, Biomechanics and thermodynamics of nanoparticle interactions with plasma and endosomal membrane lipids in cellular uptake and endosomal escape, Langmuir 30 (2014) 7522–7532, https://doi.org/10.1021/la5015219.
[103] D. Nieciecka, A. Rękorajska, D. Cichy, P. Końska, M. Żuk, P. Krysiński, Synthesis and characterization of magnetic drug carriers modified with Tb3+ ions, Nanomaterials 12 (2022) 795, https://doi.org/10.3390/nano12050795.
[104] D. Nieciecka, J. Celej, M. Żuk, A. Majkowska-pilip, K. Żelechowska-matysiak, A. Lis, M. Osial, Hybrid system for local drug delivery and magnetic hyperthermia based on SPIONs loaded with doxorubicin and epirubicin, Pharmaceutics 13 (2021), https://doi.org/10.3390/pharmaceutics13040480.
[105] R.M. Kavasi, C.C. Coelho, V. Platania, P.A. Quadros, M. Chatzinikolaidou, In vitro biocompatibility assessment of nano-hydroxyapatite, Nanomaterials 11 (2021) 1–15, https://doi.org/10.3390/nano11051152.
[106] M. Motskin, D.M. Wright, K. Muller, N. Kyle, T.G. Gard, A.E. Porter, J.N. Skepper, Hydroxyapatite nano and microparticles: correlation of particle properties with cytotoxicity and biostability, Biomaterials 30 (2009) 3307–3317, https://doi.org/10.1016/j.biomaterials.2009.02.044.
[107] Z. Shi, X. Huang, Y. Cai, R. Tang, D. Yang, Size effect of hydroxyapatite nanoparticles on proliferation and apoptosis of osteoblast-like cells, Acta Biomater. 5 (2009) 338–345, https://doi.org/10.1016/j.actbio.2008.07.023.
[108] N. Montazeri, R. Jahandideh, E. Biazar, Synthesis of fluorapatite-hydroxyapatite nanoparticles and toxicity investigations, Int. J. Nanomed. 6 (2011) 197–201, https://doi.org/10.2147/ijn.s15461.
[109] B. Du, L. Jiang, L. Zhong, Synergistic inhibitory effects of curcumin and 5-fluorouracil on the growth of the human colon cancer cell line HT-29, Chemotherapy 52 (2006) 23–28, https://doi.org/10.1159/000090238.

[110] M. Shakibaei, P. Kraehe, B. Popper, P.S. Shayan, A. Goel, C. Buhrmann, Curcumin potentiates antitumor activity of 5-fluorouracil in a 3D alginate tumor microenvironment of colorectal cancer, BMC Cancer 15 (2015) 250, https://doi.org/10.1186/s12885-015-1291-0.

[111] M. Shakibaei, C. Buhrmann, P. Kraehe, P.S. Shayan, C. Lueders, A. Goel, Curcumin chemosensitizes 5-fluorouracil resistant MMR-deficient human colon cancer cells in high density cultures, PLoS One 9 (1) (2014), e85397, https://doi.org/10.1371/journal.pone.0085397.

[112] W. Ni, Z. Li, Z. Liu, Y. Ji, L. Wu, S. Sun, X. Jian, X. Gao, Dual-targeting nanoparticles: codelivery of curcumin and 5-fluorouracil for synergistic treatment of hepatocarcinoma, J. Pharmaceut. Sci. 108 (3) (2019) 1284–1295, https://doi.org/10.1016/j.xphs.2018.10.042.

[113] V.A. Arzumanian, O.I. Kiseleva, E.V. Powerennaya, The Curious Case of the HepG2 cell line: 40 years of expertise, Int. J. Mol. Sci. 4 (23) (2021), 13135, https://doi.org/10.3390/ijms222313135.

[114] A. Dhanavel, T.A. Revathy, T. Sivaranjani, V. Narayanan, A. Stephen, 5-Fluorouracil and curcumin co-encapsulated chitosan/reduced graphene oxide nanocomposites against human colon cancer cell lines, Polym. Bull. 77 (2020) 213–233, https://doi.org/10.1007/s00289-019-02734-x.

[115] V. Ciaffaglione, M.N. Modica, V. Pittalà, G. Romeo, L. Salerno, S. Intagliata, Mutual prodrugs of 5-fluorouracil: from a classic chemotherapeutic agent to novel potential anticancer drugs, ChemMedChem 16 (23) (2021) 3496–3512, https://doi.org/10.1002/cmdc.202100473.

[116] X. Bai, Z.L. Smith, Y. Wang, S. Butterworth, A. Tirella, Sustained drug release from smart nanoparticles in cancer therapy: a comprehensive review, Micromachines 13 (2022) 1–54, https://doi.org/10.3390/mi13101623.

[117] S.A.A. Rizvi, A.M. Saleh, Applications of nanoparticle systems in drug delivery technology, Saudi Pharmaceut. J. 26 (2018) 64–70, https://doi.org/10.1016/j.jsps.2017.10.012.